NASA Technical Memorandum 87757

COMPARISON OF EXPERIMENTAL SURFACE PRESSURES WITH THEORETICAL PREDICTIONS ON TWIN TWO-DIMENSIONAL CONVERGENT-DIVERGENT NOZZLES

JOHN R. CARLSON, ODIS C. PENDERGRAFT, JR.,
AND JAMES R. BURLEY, II

AUGUST 1986

National Aeronautics and
Space Administration

Langley Research Center
Hampton, Virginia 23665

SUMMARY

A three-dimensional subsonic aerodynamic panel code (VSAERO) was used to predict the effects of upper and lower external nozzle flap geometry on the external afterbody/nozzle pressure coefficient distributions and external nozzle drag of nonaxisymmetric convergent-divergent exhaust nozzles having parallel external sidewalls installed on a generic twin-engine high performance aircraft model. Nozzle static pressure coefficient distributions along the upper and lower surfaces near the model centerline and near the outer edges (corner) of the two surfaces were calculated, and nozzle drag was predicted using these surface pressure distributions. A comparison between the theoretical predictions and experimental wind tunnel data is made to evaluate the utility of the code in calculating the flow about these types of non-axisymmetric afterbody configurations.

For free-stream Mach numbers of 0.60 and 0.90, the conditions where the flows were attached on the boattails yielded the best comparison between the theoretical predictions and the experimental data. For the boattail terminal angles of greater than 15^{0}, the experimental data for M = 0.60 and 0.90 indicated areas of separated flow, so the theoretical predictions failed to match the experimental data. Even though calculations of regions of separated flows are within the capabilities of the theoretical method, acceptable solutions were not obtained.

INTRODUCTION

Recent studies (ref. 1-12) of nonaxisymmetric nozzles have shown potential improvements in aircraft performance and effectiveness especially with the incorporation of thrust vectoring and reversing into the nozzle concept. It is also understood from these references that once non-axisymmetric nozzles are incorporated into an aircraft concept, thrust vectoring and thrust reversing can be added with only a minor weight penalty. Thrust vectoring and reversing, by virtue of its potential for enhanced aircraft capability, may be a requirement for the next generation fighter aircraft. If these nozzles are to be utilized they must be integrated into the aircraft in such a way as to either reduce the aircraft drag or maintain the drag at levels associated with current axisymmetric nozzles. A number of studies have been undertaken to determine the most efficient method for integrating non-axisymmetric nozzles into twin engine fighter aircraft. The development and utilization of advanced computational methods will play a vital role in developing this technology. As a result the current form of research activities at the Langley Research Center is to develop the data base for new non-axisymmetric nozzle concepts, as well as, to develop and validate computational methods for predicting the flow characteristics on these nozzles.

The results of an investigation to determine the external drag characteristics of non-axisymmetric twin engine type afterbody/nozzle shape has been reported in reference 13. In this reference the effects of upper and lower external nozzle flap geometry on the afterbody and external nozzle pressure coefficient distributions, afterbody forces and moments, and integrated nozzle axial force are presented. The nozzle flap geometry was formed by a parametric combination of circular arcs and

straight lines with the nozzle external sidewalls having parallel surfaces. For this report, the experimental data for configurations 2, 5, 13, 14, and 21 at M = 0.60 and M = 0.90 at an angle-of-attack of zero degrees ($\alpha = 0^0$) and operating nozzle pressure ratios (NPR) from jet-off to 8 are compared to the theoretical predictions of the vortex separation aerodynamic program (VSAERO) detailed in references 14 and 15. These configurations offer a comparison between nozzles of the same length with varying terminal boattail angle, nozzles of the same terminal boattail angle with varying circular arc fairing radii, and one very short steep boattail profile.

VSAERO is a surface singularity program using quadrilateral panels to represent arbitrary three-dimensional bodies. This code includes such features as wake shape iteration, jet-wakes, on and off body stream line calculations, viscous/inviscid interactions and off-body velocity calculations. Other features include modeling of jet exhaust and separated wakes and calculating the effects of flow separation and boundary layer growth. This code was used to calculate the external static pressure coefficient distributions and nozzle drag coefficients for the subject nozzle/afterbodies. The results are then compared to the experimental data of reference 13 to assess the capabilitiy of the code to predict 2-D C-D afterbody/nozzle external flows and external drag.

SYMBOLS

Model forces and moments are referenced to the stability-axis system with the model reference center located at $0.25\bar{c}$, which corresponds to fuselage station (FS) 36.09 inches and 1.75 inches above the model centerline. All aerodynamic coefficients are nondimensionalized with respect to $q_\infty S$ or $q_\infty S\bar{c}$.

C_D	drag coefficient, $D/q_\infty S$
$C_{D,aft}$	afterbody drag coefficient
$C_{D,n}$	nozzle drag coefficient
c_p	pressure coefficient, $\frac{p-p_\infty}{q_\infty}$
$\bar{c}$	wing mean geometric chord, 17.47 in.
ι	length, in.
M, MACH	Mach number
p	surface static pressure, psi
p_∞	free-stream static pressure, psi
q_∞	free-stream dynamic pressure, psi
R	radius, in.
S	wing reference area, 664 in^2
W	width, in.

x, X	distance downstream from FS 66.54
y	spanwise distance from model centerline, in.
α, ALPHA	model angle of attack, deg
β	boattail angle, deg
Subscripts:	
A	afterbody
c	chord
e	nozzle exit
f	flap
i	arc/straight line tangent point
n, N	nozzle
o	circular arc center
t	throat location or terminal angle
Abbreviations	
A/B	afterburning
BL	butt line
Conf.	configuration
FS	fuselage station
NPR	nozzle pressure ratio, $p_{t,j}/p_\infty$
WL	water line
2-D C-D	two-dimensional convergent-divergent

EXPERIMENTAL DATA AND THEORETICAL METHOD

Wind Tunnel

The experimental investigation of reference 13 was conducted in the Langley 16-Foot Transonic Tunnel, a single-return, continuous flow, atmospheric-pressure wind tunnel with a slotted, octagonal test section and continuous air exchange for cooling. The wind tunnel has a variable airspeed up to a Mach number of 1.30. Test section plenum suction is used for speeds above a Mach number of 1.05. A complete

description of this facility, its related equipment, and its operating characteristics can be found in references 16 and 17.

Model and Tests

A sketch of the wing-tip supported model with a typical nozzle installed is shown in figure 1(a) with details of the jet simulation system and balance arrangement. The overall model arrangement represents a twin engine fighter with tail surfaces removed and faired over, twin side inlets. Figure 1(b) is a half span sketch showing the wing planform geometry and model reference moment center. The wing was mounted 1.75 inches above the model centerline, had an aspect ratio of 2.40, a taper ratio of 0.43, and a NACA 64-series airfoil section with thickness ratio of .067 near the root. The outboard area of the wing had increased thickness ratio (0.10 at the tip) for structural support and for compressed air and instrumentation passages. The wing/centerbody together with the twin support booms, formed the bifurcated-sting model support system. A complete description of this support system and the various balance arrangements that may be used can be found in references 6 and 16, and further description of the arrangement used in these particular tests may be found in reference 13.

Photographs of the model installed in the test section of the Langley 16-Foot Transonic Tunnel are presented in figure 2.

The twin-engine afterbody shown in figure 3(a) and 3(b) was designed to be representative of current fighter aircraft, while housing the propulsion simulation system, afterbody balance, and related static pressure tubes from the nozzles and afterbody. The afterbody is constant in width so that all closure is accounted for on the top and bottom surfaces using a 5^{o} boattail between FS 59.19 and the end of the afterbody at FS 66.04 (see figure 3(a)).

Figure 4(a) presents a sketch and table giving geometry of the two-dimensional convergent-divergent (2-D C-D) nozzle models tested. Of the 21 configurations shown in the table and reported in reference 13, only the 5 indicated by the + sign in the configuration column are used in this paper. The five configurations selected are dry power configurations using identical internal nozzle geometry.

An external high-pressure air supply system provided the nozzles with a continuous flow of clean dry air at a controlled temperature of 70^{o}F. The air was used to simulate exhaust flow over a range of nozzle pressure ratios (NPR's) from about 1.0 (jet off) up to about 10.0 depending on Mach number.

Figure 4(b) shows the locations for the 23 static pressure orifices on the top flap, and the 11 orifices on the bottom flap of each nozzle. Each orifice number was located at the same ratio of nozzle length (x/l_n), regardless of nozzle configuration.

The external static pressure orifice data on the right-hand nozzle were used to compute external forces and moments on the entire nozzle by a numerical summation of the local nozzle static-pressure coefficient multiplied by a projected area assigned to each of the orifices on the nozzle and all divided by the reference area. Flow on the model was assumed to be symmetrical right to left, so each orifice was assigned both right and left side areas appropriate to the particular orifice. Normal and axial projected areas were used to compute drag coefficient data.

Model angle of attack was computed from an attitude indicator located inside of one of the boom fairings, and corrected for 0.1^{o} flow angularity, which is the average flow angle measured in the 16-Foot Transonic tunnel.

The investigation of reference 13 was conducted in the Langley 16-Foot Transonic Tunnel at free-stream Mach numbers of 0.60, 0.70, 0.80, 0.90, and 1.20. The nozzle pressure ratio was varied from 1.0 (jet off) to 10.0, depending on free-stream Mach number. For this report, only data for M = 0.60 and M = 0.90 at $\alpha = 0^{o}$ are used with NPR set at typical operating values for each Mach number.

VSAERO Theoretical Prediction Method

VSAERO (Vortex Separation Aerodynamic Program) is a surface singularity solution to the Laplace equation using quadrilateral panels to represent arbitrary three-dimensional bodies. Source and doublet singularities are distributed in a piecewise constant fashion on each panel. Neumann boundary conditions are applied to the panel to determine the singularity strength. Dirichlet boundary conditions are applied at the boundary to determine the doublet strength. More detailed discussions of the method appear in references 14 and 15.

The code includes features such as wake shape iteration, jet exhaust, on- and off-body streamline calculations, and off-body velocity calculations. Jet wakes, in particular, are modeled using doublet sheets with a linear variation in doublet strength in the streamwise direction. Jet exhaust flow can be modeled by specifying a unit normal velocity outflow at the exhaust. The major limitation in the use of the code, is the incompressible nature of the basic equation. However, transonic results may be approximated through the use of the Prandtl-Glauert compressibility correction. The VSAERO code is capable of modeling the full geometry of the 2-D C-D model configurations including body, wing, exhaust nozzle, and wing-tip support booms.

The geometrical description of the various configurations is based on panels, patches, and wakes, which can be combined to form components and assemblies. Some automatic capabilities are provided in the code for paneling and also patch generation in special situations. The computed geometrical description of the 2-D C-D afterbody model is shown in figure 5 as produced from data input to the VSAERO code.

The effects of viscosity are calculated using a two-dimensional, integral boundary layer calculation (ref. 18). The calculations follow surface streamlines that have been determined from an initial potential flow calculation. The boundary layer thickness from this calculation is simulated by surface transpiration, and a new potential calculation is performed using the transpiration velocities.

Typical computational times for the 2-D C-D boattail model using approximately 1100 panels and running 6 to 8 boundary layer iterations were 4 hours on a MicroVAX II.

RESULTS AND DISCUSSION

Nozzle Pressure Distribution

Static-pressure-coefficient distributions on the external surface of the nozzle boattail are presented in figure 6 for M = 0.60 data and figure 7 for M = 0.90 data for configurations 2, 5, 13, 14, and 21 of table 4(a). All data are for a zero angle-of-attack and symbols are used to indicate the experimentally determined nozzle-pressure distributions. The location of the rows of orifices on the boattail are shown in figure 4(b). Theoretical pressure distributions computed are presented in figures 6 and 7 as solid lines.

Comparisons at M = 0.60.- In general, the agreement of the theoretical and experimental pressure distributions are good (see figure 6). Typical nozzle boattail pressure distributions are characterized at subsonic speeds by an expansion near the start of the boattail followed by a pressure recovery on the remaining portion of the boattail ($x_n/l_n = 0$) . The degree of flow expansion depends upon the rate of change of slope between the model afterbody and the nozzle boattail at the nozzle connect station.

The degree of pressure recovery depended upon the nozzle pressure ratio, free-stream Mach number and, to some degree, upon proximity to the nozzle external sidewall. The theoretical method predicted the degree of initial flow expansion for configurations in which the slope transition from afterbody to nozzle boattail was small or a circular-arc fairing (see figure 6(a) for example). Little or no flow separation at the start of the boattail, i.e., x_n/l_n = -0.2 to +0.2, was evident for even the shortest and steepest nozzle, configuration 5. Poor agreement occurred at the nozzle corner near the sidewall, i.e., rows 4 and 5 for all nozzle concepts. Also, poor agreement occurred at the nozzle trailing edge where jet entrainment and plume blockage effects tend to dominate the flow. For these calculations, the shape of the simulated jet wake was allowed to relax to assume a shape determined by the pressures calculated by the initial potential flow solutions. This new shape was used for any subsequent viscous and inviscid flow solutions. The jet wake relaxation could account for some part of a plume blockage effect. Jet entrainment effects were not included in these calculations, though a type of entrainment modeling was within the capability of the code. The predicted spanwise variation of the level of pressure recovery, by comparing the point x_n/l_n = .9 for rows 1 through 4, was greater than that for the experimental data. This slight mismatch in the comparison is caused by a lack of accurate plume modeling. The poorest agreement, overall, occurred for configuration 5 (see figure 6(b)) in the region of apparent flow separation, x_n/l_n = 0.5 to 1.0 for rows 1 and 2. Though separated wake modeling was also a capability of the code, a reasonable and stable solution utilizing that modeling was not obtained. This modeling problem was likely due to insufficient damping of the flow solution in the separated flow region between each boundary-layer iteration. In addition, the area of flow separation appeared irregular in shape, i.e., not along a fixed row or column of the paneled geometry, thus subsequently making a good separated flow solution difficult to obtain.

Changes in the pressure coefficient distribution with variation in nozzle cross-section shape were predicted well. Abrupt changes in surface curvature were particularly noticeable in the configurations with combination circular arc-straight line shape cross-sections. Configuration 14, figure 6(d) and 7(d), at x_n/l_n = .4 and configuration 21, figure 6(e) and 7(e), at x_n/l_n = 0.05, both show discontinuities in the pressure coefficient distributions due to change in surface

curvature. Though it was difficult to assess the accuracy of the predicted magnitude of the expansion peak, the experimental data bracketing this region are matched fairly well.

Comparisons at M = 0.90.- Overall, the observations made for the comparisons at M = 0.60, held for M = 0.90 (see figure 7) due to the external flow expansion, and following recompression remained subsonic and attached for all configurations except configuration 5. All solutions computed for M = 0.90 were for inviscid flow due to convergence problems with the boundary-layer iteration scheme at this Mach number. The slope discontinuity at the connect station of configuration 5 (fig. 7(b)) was sufficient to cause flow separation off the surface of the boattail. Therefore, there was poor agreement of the predicted pressure coefficients with the experimental data. The inviscid attached flow solution greatly over-predicted the initial flow expansion about the start of the boattail and over-predicted the subsequent flow recompression. The largest discrepancy between the theoretical and experimental data occur in the region of the nozzle trailing edge where jet and viscous effects are predominant.

Drag Comparison

Theoretically predicted afterbody/nozzle drag coefficient, and experimental drag coefficient for M = 0.6 and M = 0.90 are compared in figure 8. The discussion will be limited to that of the 10^{o} nozzle terminal boattail angle configurations; 2, 14, and 21. The major difference in the boattail longitudinal shape between these three configurations was the radius of curvature of the circular arc, fairing the flat portion of the nozzle to the afterbody, i.e. column heading R in table 4(a). As indicated by the sketch at the top of figure 8, nozzle drag coefficient is indicated by an open bar and afterbody drag coefficient by a cross hatched bar, and the total afterbody/nozzle drag coefficient by the arrow. Configuration number is indicated at the bottom of each bar. As you can see from these data the integrated pressure distributions on the afterbody and nozzle do not agree with the measured drag data. This can be attributed to the fact that the pressure drag was calculated by the area-pressure integration procedure which always yields some inaccuracies simply because an adequate number of measurements is difficult to obtain.

The prediction of the lowest afterbody drag, configuration 14, agreed with the experimental test data for both Mach numbers, though the absolute level of drag was considerably underpredicted. The predicted trend of total afterbody/nozzle drag coefficient for the three configurations did not agree with the test data at either Mach number. Different trends in the nozzle drag coefficient occur at M = 0.6 comparing the theory with experimental data. At M = 0.9, the degree of change in afterbody drag coefficient due to changing nozzle shape was sufficient to cause the disagreement in the total drag trends. A partial reason for this discrepancy can be explained by the fact that the experimentally determined nozzle pressure drag was calculated by the area-pressure integration procedure. The arrangement of the orifices used for the integration and the number of orifices used can introduce some error into the calculation. For this set of nozzles, there were no pressure data obtained for the outboard 10 percent of the nozzle planform. It is interesting to note that the theoretical predictions show the corner region to be an area of positive drag, as shown in figure 9. This figure is a plot of integrated pressure drag along lines of constant span, moving from the nozzle boattail centerline to the sidewall. It appears that the central 90 percent of the boattail surface contributes a negative drag component to the total drag of the nozzle. The strong

corner flow turning from the sidewall onto the upper and lower external nozzle flaps induce negative pressures in this region, resulting in the positive drag component. The magnitude of this additional drag did not change significantly between the three configurations, and may account for the differences in the level of drag of each nozzle (between theory and the experimental data) but not the trend of drag change between each nozzle.

CONCLUSIONS

A three-dimensional subsonic aerodynamic panel code (VSAERO) was used to predict the effects of external nozzle flap geometry on the external afterbody/nozzle drag of nonaxisymmetric convergent-divergent exhaust nozzles having parallel external sidewalls installed on a generic twin-engine high performance aircraft model. External geometries for 5 configurations were used to evaluate the utility of the code. A comparison of the static pressure coefficients predicted on the nozzle boattail with the experimental data and a comparison of afterbody/nozzle drag coefficients result in the following conclusions:

1. Good prediction of the flow about afterbody/nozzle configurations can be made, except in cases of separated or supersonic flows. The computational code did predict the occurrance of flow separation, however a converged solution of the separated flow was not obtained.

2. Prediction of total afterbody/nozzle drag trends did not agree with the experimental data. The incremental changes in drag coefficient for both the experimental data and the theoretical predictions were small. A clear advantage of one configuration over another was difficult to discern.

REFERENCES

1. Pendergraft, O. C., Jr.: Comparison of Axisymmetric and Non-Axisymmetric Nozzles Installed on the F-15 Configuration. AIAA Paper No. 77-842, July 1977.

2. Berrier, Bobby L.; Palcza, J. Lawrence; and Richey, G. Keith: Nonaxisymmetric Nozzle Technology Program - An Overview. AIAA Paper No. 77-1225, Aug. 1977.

3. Stevens, H. L.: F-15/Nonaxisymmetric Nozzle System Integration Study Support Program. NASA CR-135252, 1978.

4. F-15 2-D Nozzle System Integration Study. Volume I - Technical Report. NASA CR-145295, 1978.

5. Capone, Francis J.: The Nonaxisymmetric Nozzle - It is for Real. AIAA Paper 79-1810, Aug. 1979.

6. Yetter, Jeffery A.; and Leavitt, Laurence D.: Effects of Sidewall Geometry on the Installed Performance of Nonaxisymmetric Convergent-Divergent Exhaust Nozzles. NASA TP-1771, 1980.

7. Stevens, H. L.; Thayer, E. B.; and Fullerton, J. F.: Development of the Multi Function 2-D/C-D Nozzle. AIAA Paper 81-1491, July 1981.

8. Capone, F. J.; Hunt, B. L.; and Poth, G. E.: Subsonic/Supersonic Nonvectored Aeropropulsive Characteristics of Nonaxisymmetric Nozzles Installed on an F-18 Model. AIAA Paper 81-1445, July 1981.

9. Nelson, B. D.; and Nicolai, L. M.: Application of Multi-Function Nozzles to Advanced Fighters. AIAA Paper 81-2618, Dec. 1981.

10. Re, Richard J. and Leavitt, Laurence D.: Static Internal Performance Including Thrust Vectoring and Reversing of Two-Dimensional Convergent-Divergent Nozzsles. NASA TP-2253, 1984.

11. Carson, George T., Jr.; Capone, Francis J.; and Mason, Mary L.: Aeropropulsive Characteristics of Nonaxisymmetric Nozzle Thrust Reversers at Mach Numbers from 0 to 1.20. NASA TP-2306, 1984.

12. Leavitt, L. D.: Summary of Nonaxisymmetric Nozzle Internal Performance from the NASA Langley Static Test Facility. AIAA Paper 85-1347, July 1985.

13. Pendergraft, Odis C., Jr.; Burley, James R., II; and Bare, E. Ann: Study of Parametric Afterbody/Nozzle Drag on Twin Two-Dimensional Convergent-Divergent Nozzles at Mach Numbers From 0.60 to 1.20. NASA TP-2640, 1986.

14. Maskew, B.: A Three-Dimensional Viscous/Potential Flow Interaction Analysis Method for Multi-Element Wings; Modifications to the Potential Flow Code to Allow Part-Span, High-Lift Devices and Close-Interference Calculations. NASA CR-152277, March 1979.

15. Maskew, B.: Prediction of Subsonic Aerodynamic Characteristics: A Case for Low-Order Panel Methods. J. Aircr., vol. 19, No. 2, February 1982, pp.157-163.

16. Peddrew, Kathryn A., Compiler: A User's Guide to the Langley 16-Foot Transonic Tunnel. NASA TM-83186, 1981.

17. Corson, Blake, Jr.; Runckel, Jack F.; and Igoe, William B.: Calibration of the Langley 16-Foot Transonic Tunnel with Test Section Air Removal. NASA TR R-423, 1974.

18. Cumpsty, N. A.; and Head, M. R.: The Calculation of Three-Dimensional Turbulent Boundary Layers, Part I: Flow Over the Rear of an Infinite Swept Wing. Aero. Quarterly, vol. XVIII, February 1967.

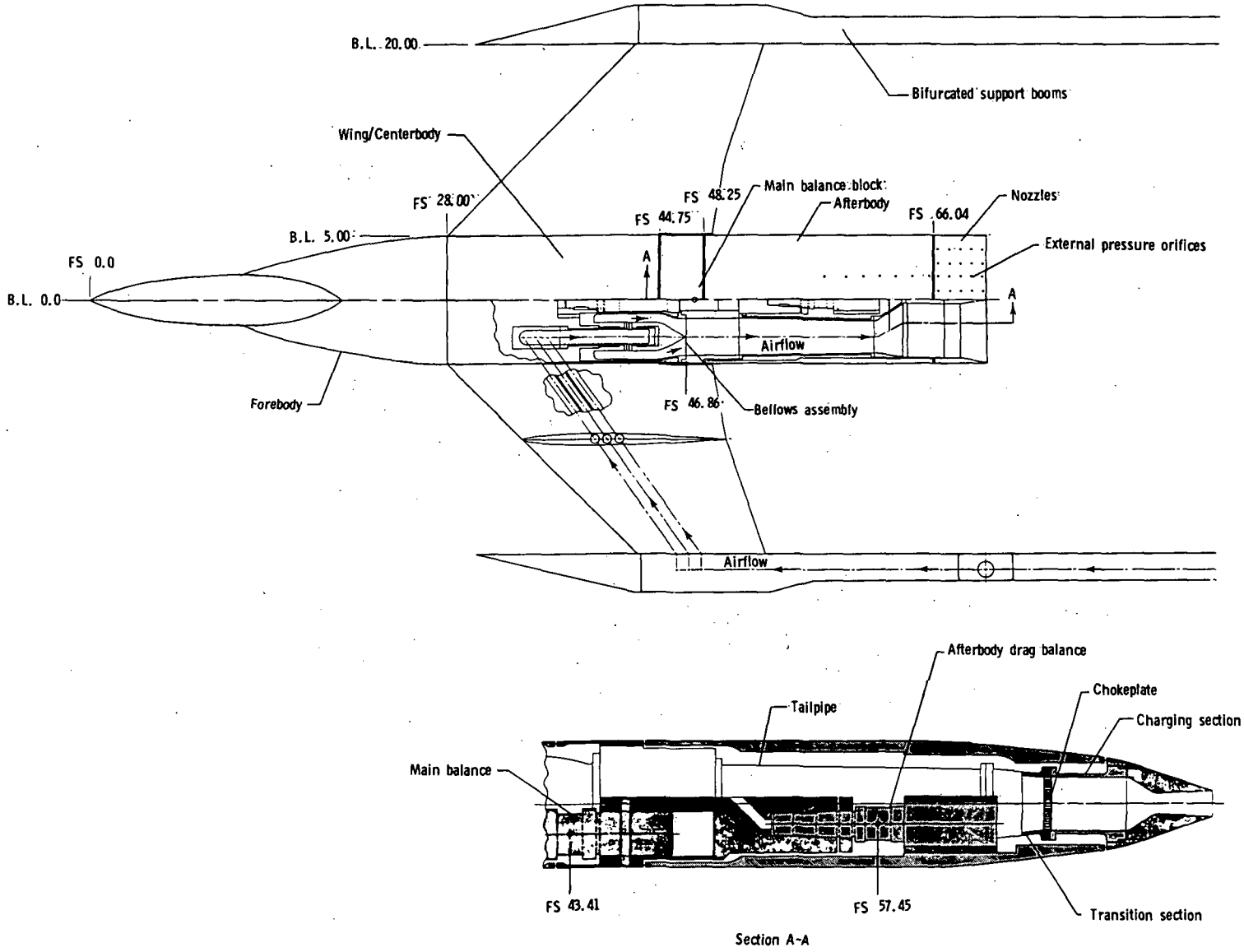

(a) Jet simulation system and balance arrangement.

Figure 1.- Sketch of air powered, twin engine, wing-tip supported model with two-dimensional convergent-divergent nozzles from reference 13. All linear dimensions in inches.

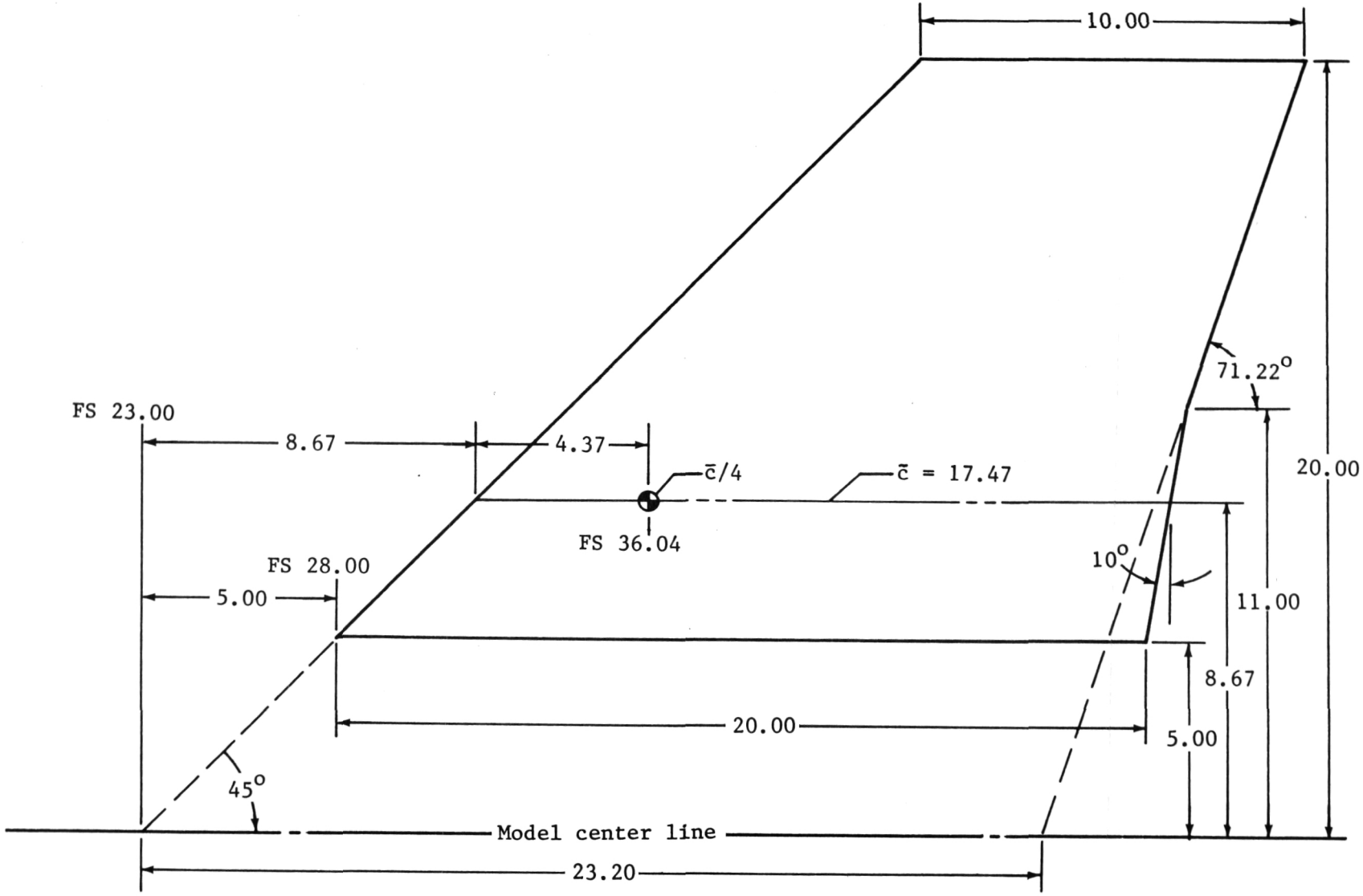

(b) Wing planform geometry.

Figure 1.- Concluded.

NASA
L-81-4090

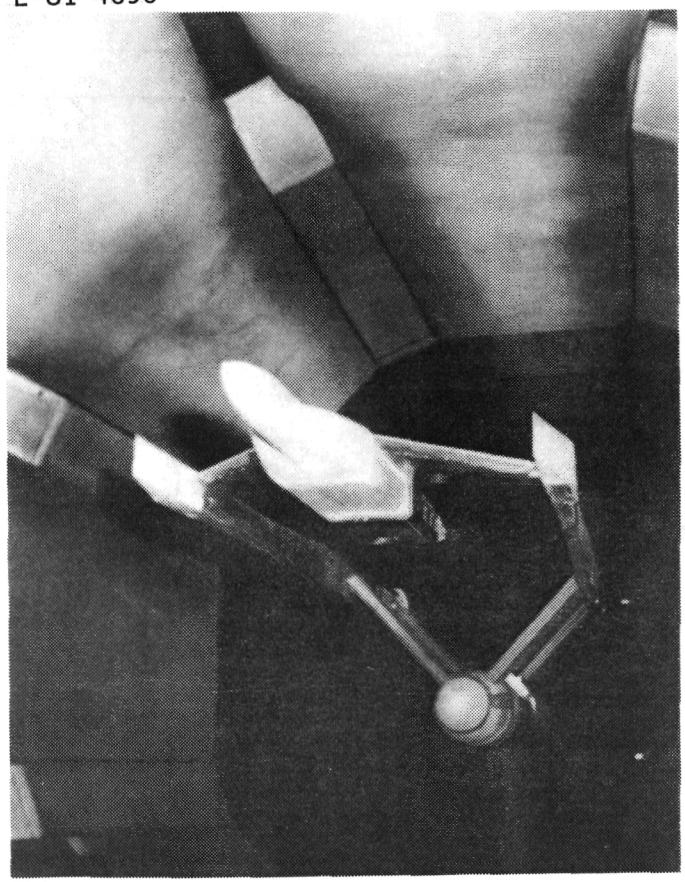

DOWNSTREAM VIEW

NASA
L-81-4089

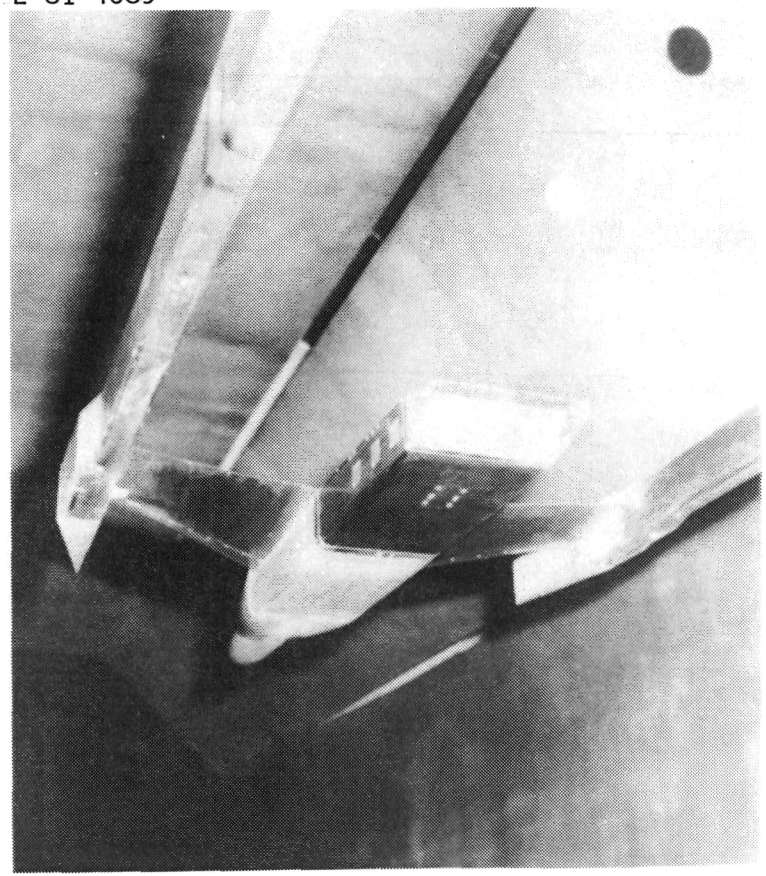

UPSTREAM VIEW

Figure 2.- Photographs from reference 13 of a two-dimensional convergent-divergent nozzle installed on the twin-engine wing-tip supported fighter model in the Langley 16-Foot Transonic Tunnel.

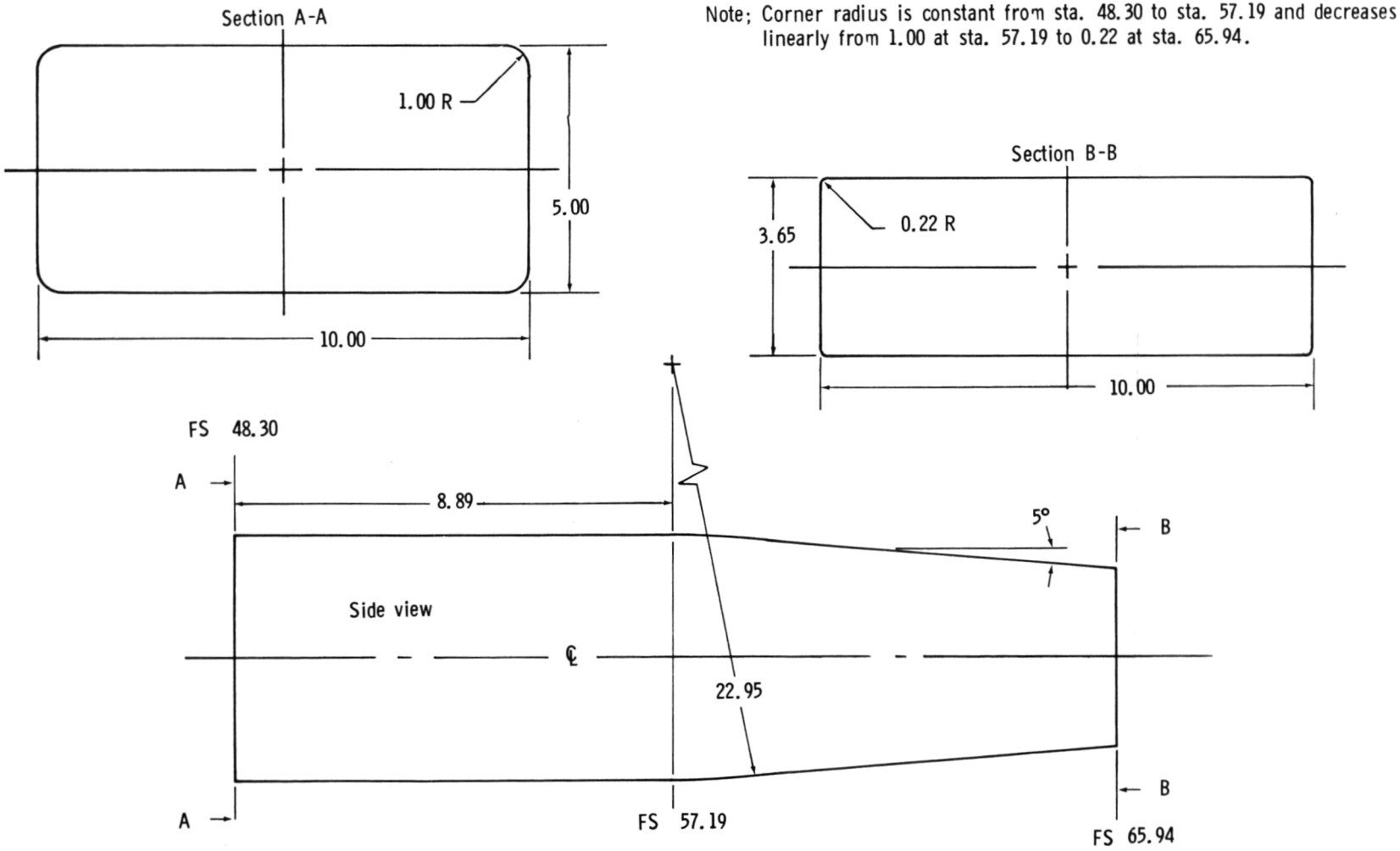

(a) Geometric details.

Figure 3.- Afterbody geometric description and static pressure orifice locations from reference 13. All linear dimensions in inches

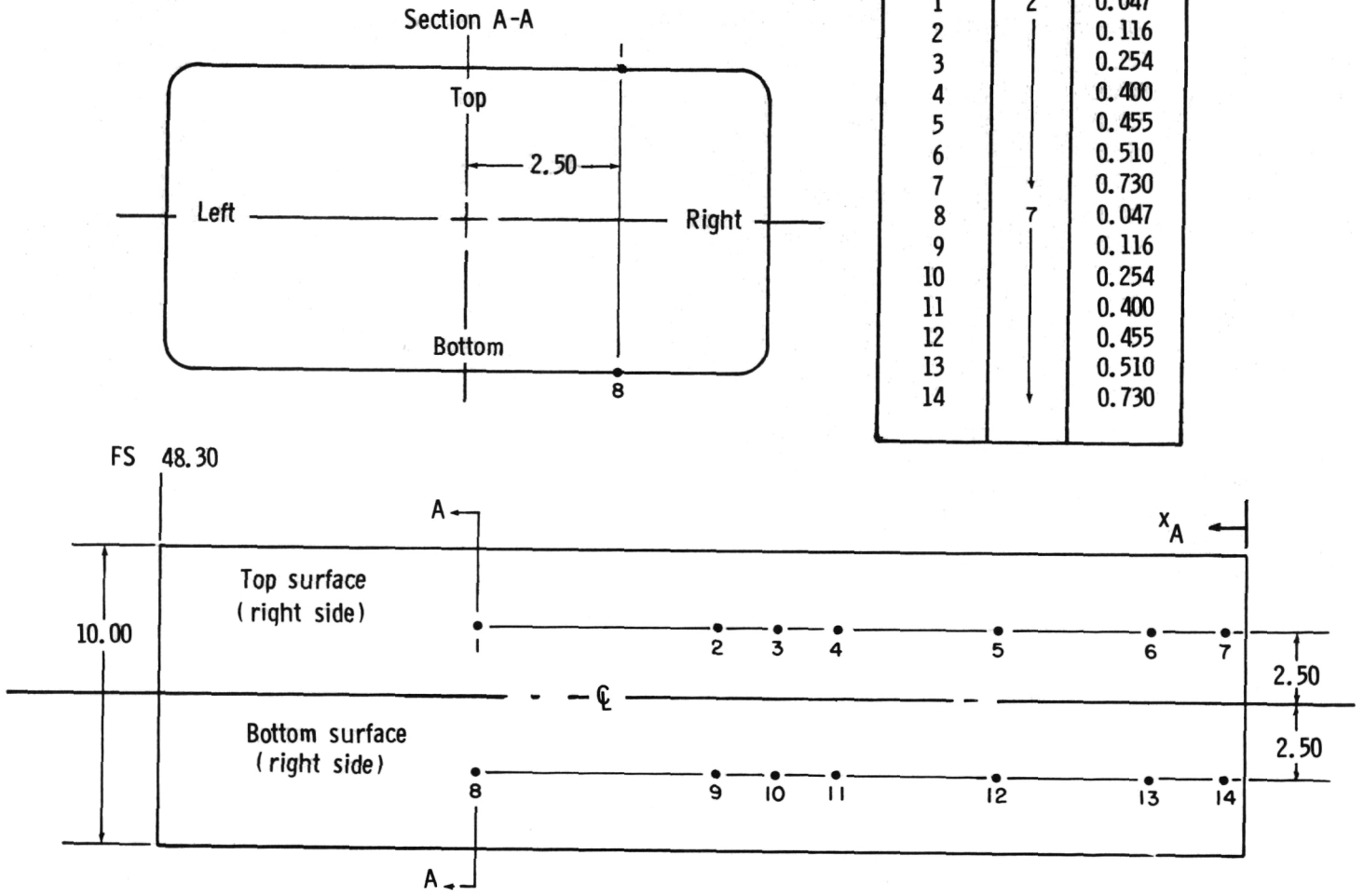

Orifice	Row	x_A/l_A
1	2	0.047
2		0.116
3		0.254
4		0.400
5		0.455
6		0.510
7		0.730
8	7	0.047
9		0.116
10		0.254
11		0.400
12		0.455
13		0.510
14		0.730

(b) Orifice locations.

Figure 3.- Concluded.

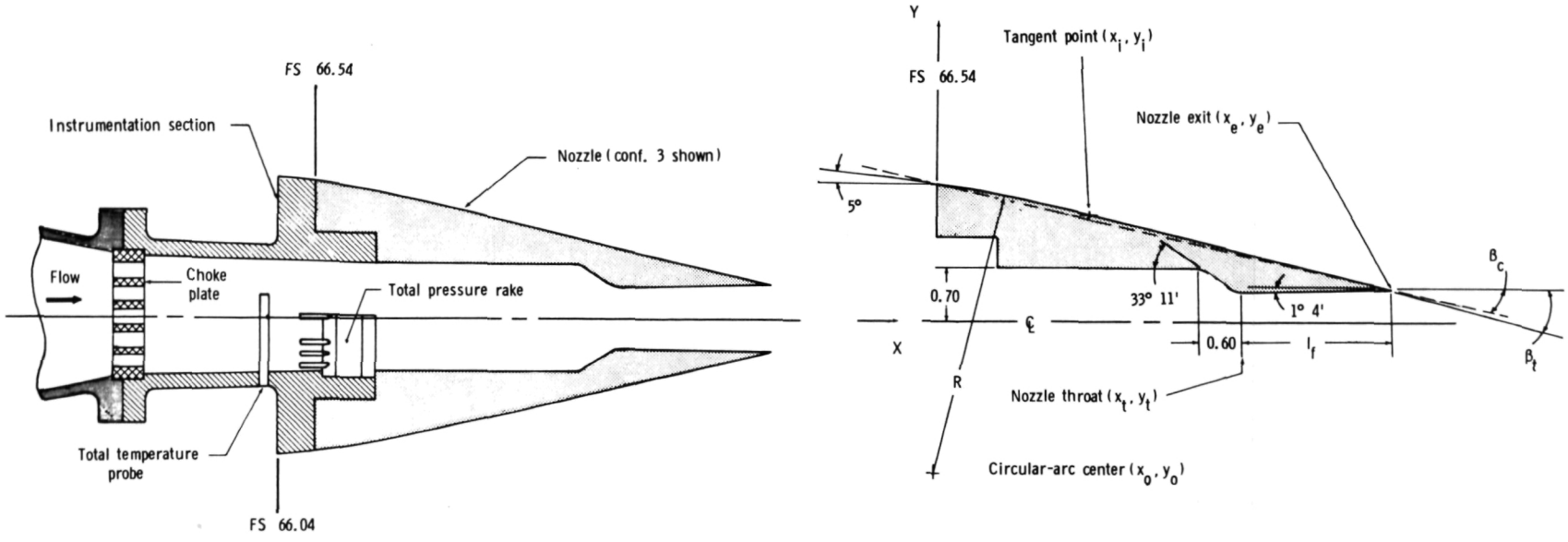

Conf	R	X_o	Y_o	X_i	Y_i	X_t	Y_t	X_e	Y_e	l_f	β_c, deg.	β_t, deg.
1	7.496	-0.653	-5.698	1.509	1.480	2.071	0.595	5.009	0.650	2.938	12.601	13.336
+ 2	0.000	0.000	1.770	0.000	1.770	5.527	0.405	7.527	0.442	2.000	10.000	10.000
3	↓	↓	↓	↓	↓	3.986	↓	5.986	↓	↓	12.500	12.500
4	↓	↓	↓	↓	↓	2.953	↓	4.953	↓	↓	15.000	15.000
+ 5	↓	↓	↓	↓	↓	1.646	↓	3.646	↓	↓	20.000	20.000
6	7.496	-0.653	-5.698	3.646	0.442	1.646	↓	3.646	↓	↓	20.000	35.000
7	↓	↓	↓	1.910	1.346	2.393	↓	4.393	↓	↓	16.810	20.000
8	↓	↓	↓	1.509	1.480	2.953	↓	4.953	↓	↓	15.000	16.760
9	14.769	-1.287	-12.983	4.953	0.442	2.953	↓	4.953	↓	↓	15.000	25.000
10	↓	↓	↓	2.534	1.322	3.819	↓	5.819	↓	↓	12.850	15.000
11	↓	↓	↓	1.407	1.578	5.527	↓	7.527	↓	↓	10.000	10.514
12	23.488	-2.057	-21.629	5.986	0.442	3.986	↓	5.986	↓	↓	12.500	20.000
+ 13	43.850	-3.822	-41.913	7.527	0.442	5.527	↓	7.527	↓	↓	10.000	15.000
+ 14	↓	↓	↓	3.792	1.270	6.488	↓	8.488	↓	↓	8.890	10.000
15	↓	↓	↓	2.127	1.532	8.081	↓	10.081	↓	↓	7.500	7.798
16	7.496	-0.653	-5.698	1.101	1.590	2.071	0.595	5.009	0.650	2.938	12.601	13.529
17	↓	↓	↓	0.679	1.679	5.527	0.405	7.527	0.442	2.000	10.000	10.234
18	23.488	-2.047	-21.629	3.037	1.302	4.914	↓	6.914	↓	↓	10.864	12.500
19	3.750	-0.327	-1.966	1.114	1.496	1.646	↓	3.646	↓	↓	20.000	22.594
20	↓	↓	↓	0.690	1.643	2.953	↓	4.953	↓	↓	15.000	15.735
+ 21	↓	↓	↓	0.331	1.726	5.527	↓	7.527	↓	↓	10.000	10.113

+ Configurations used in this comparison.

(a) Nozzle geometry.

Figure 4.- Sketches of nozzle assembly, geometric design parameters, and static pressure orifice locations on the nozzle, from reference 13. All linear dimensions in inches.

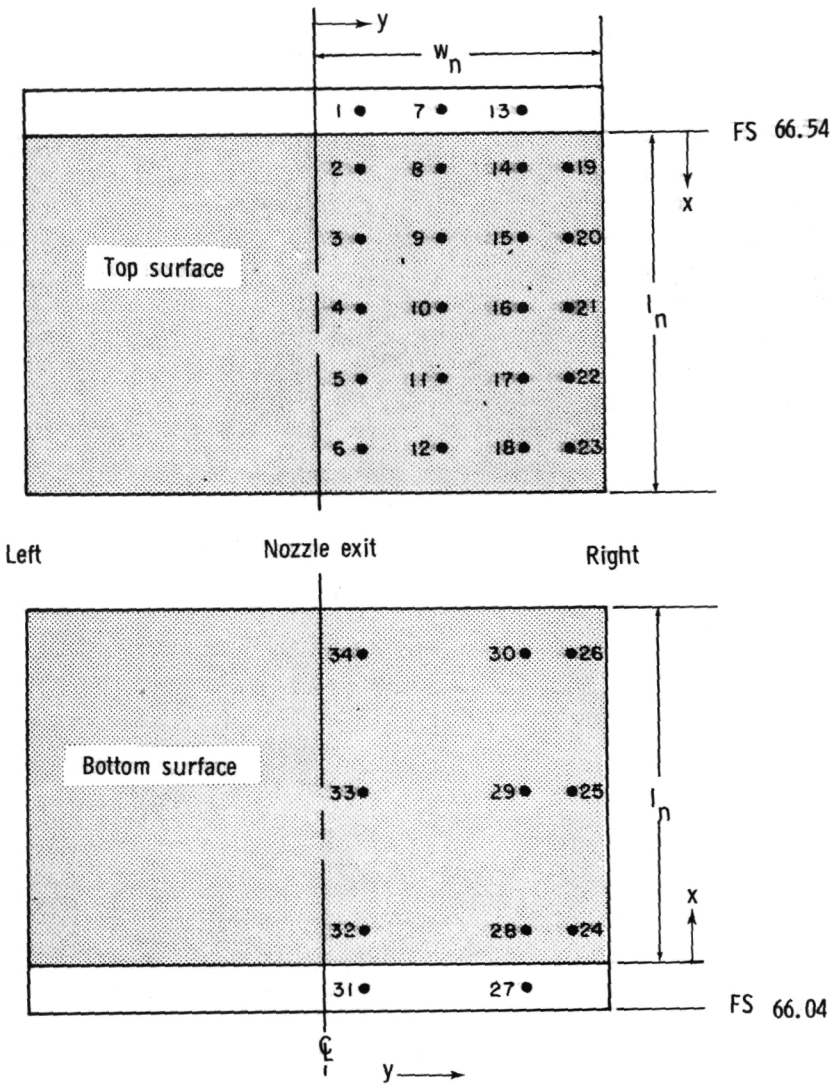

Orifice	Row	y/w_n	x/l_n
1	1	0.167	-0.0138
2			0.1
3			0.3
4			0.5
5			0.7
6			0.9
7	2	0.500	-0.0138
8			0.1
9			0.3
10			0.5
11			0.7
12			0.9
13	3	0.833	-0.0138
14			0.1
15			0.3
16			0.5
17			0.7
18			0.9
19	4	0.916	0.1
20			0.3
21			0.5
22			0.7
23			0.9
24	5		0.1
25			0.5
26			0.9
27	6	0.833	-0.0138
28			0.1
29			0.5
30			0.9
31	8	0.167	-0.0138
32			0.1
33			0.5
34			0.9

(b) Orifice locations.

Figure 4.- Concluded.

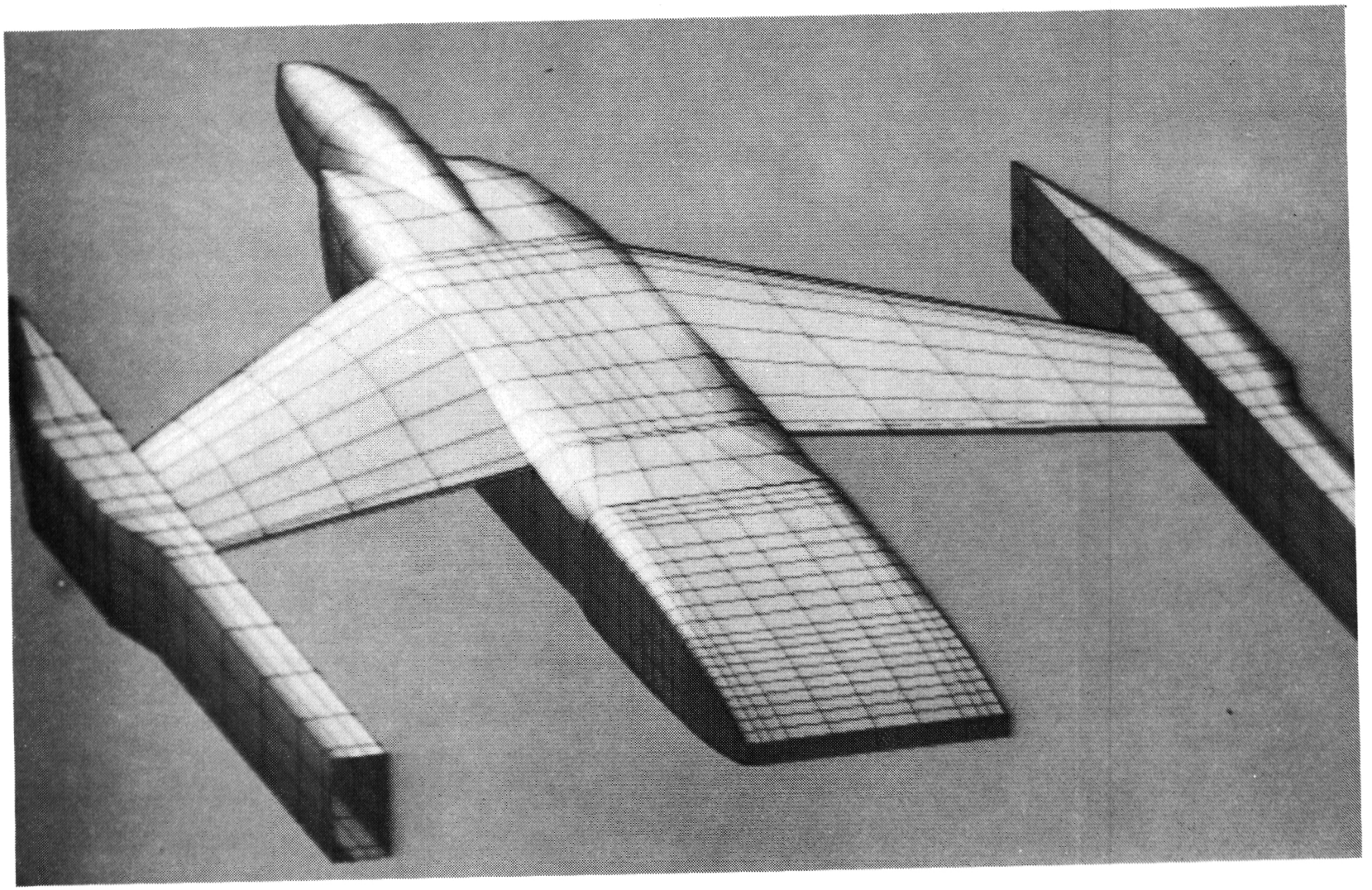

Figure 5.- Illustration of paneling of wing-tip supported afterbody model used for input to the Vortex Separation Aerodynamic Program (VSAERO).

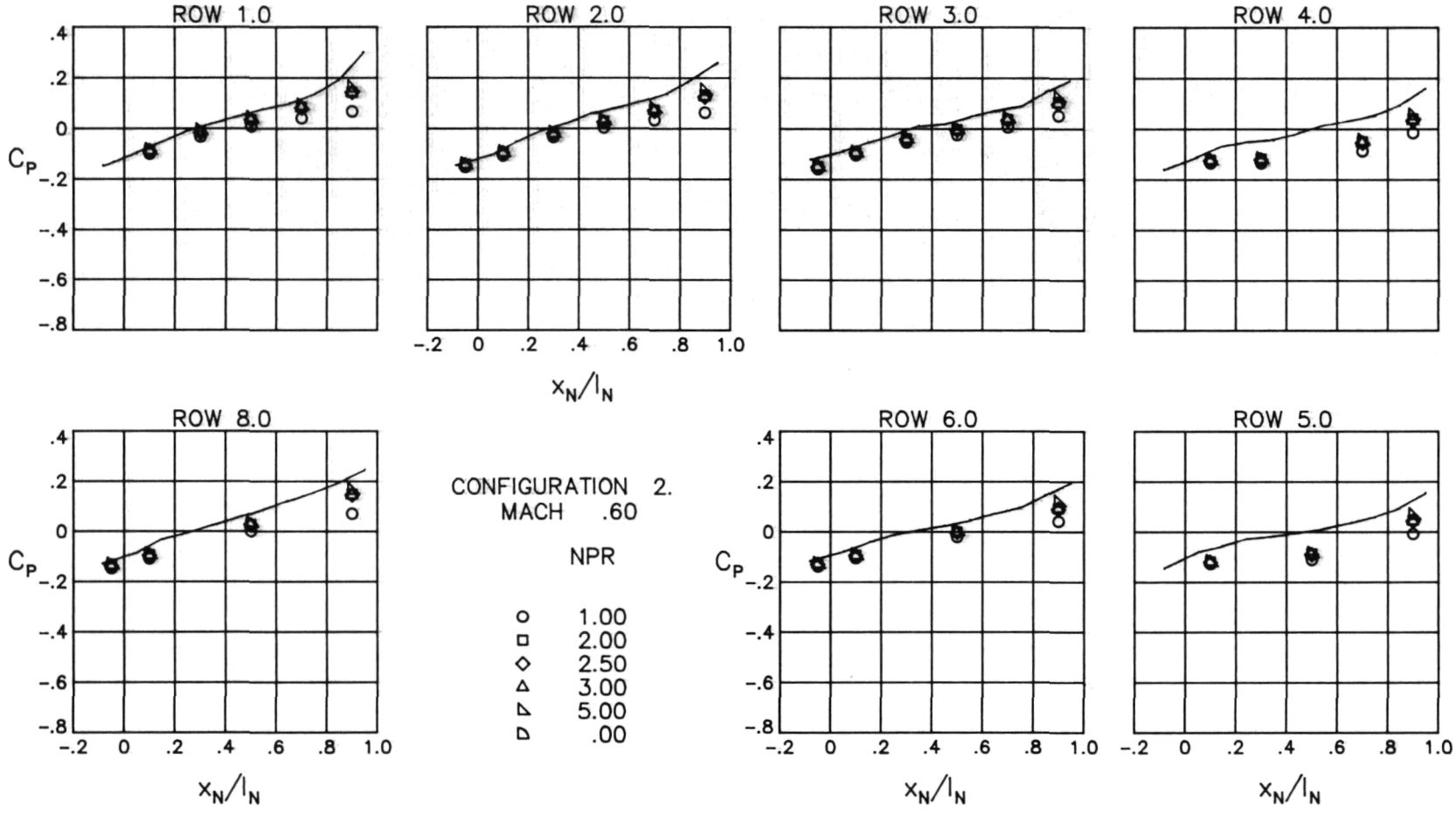

(a) Configuration 2.

Figure 6.- Surface static pressure coefficient distributions around the nozzles at M = 0.60 and $\alpha = 0^{o}$. Solid lines represent the computed values.

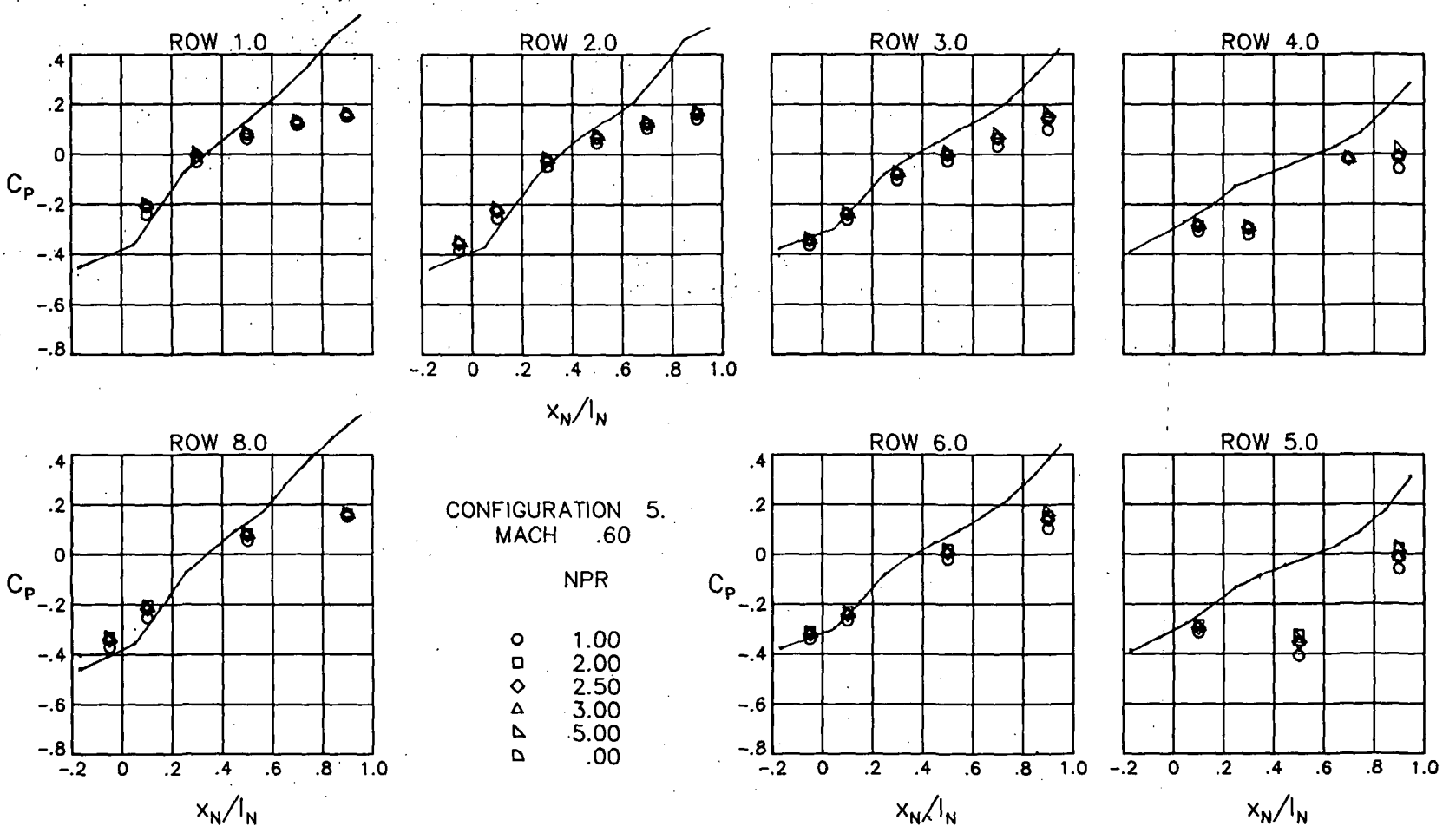

(b) Configuration 5.

Figure 6.- Continued.

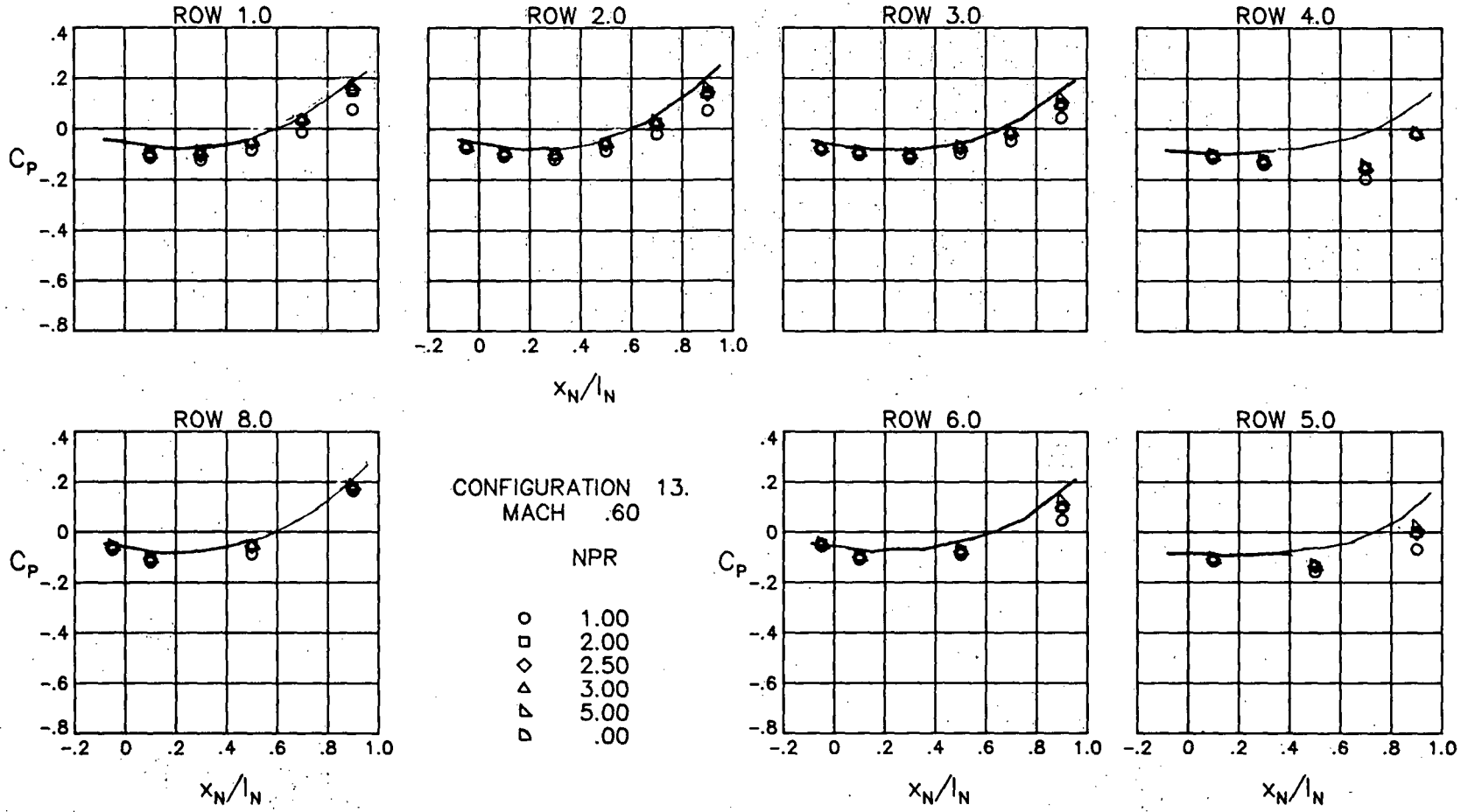

(c) Configuration 13.

Figure 6.- Continued.

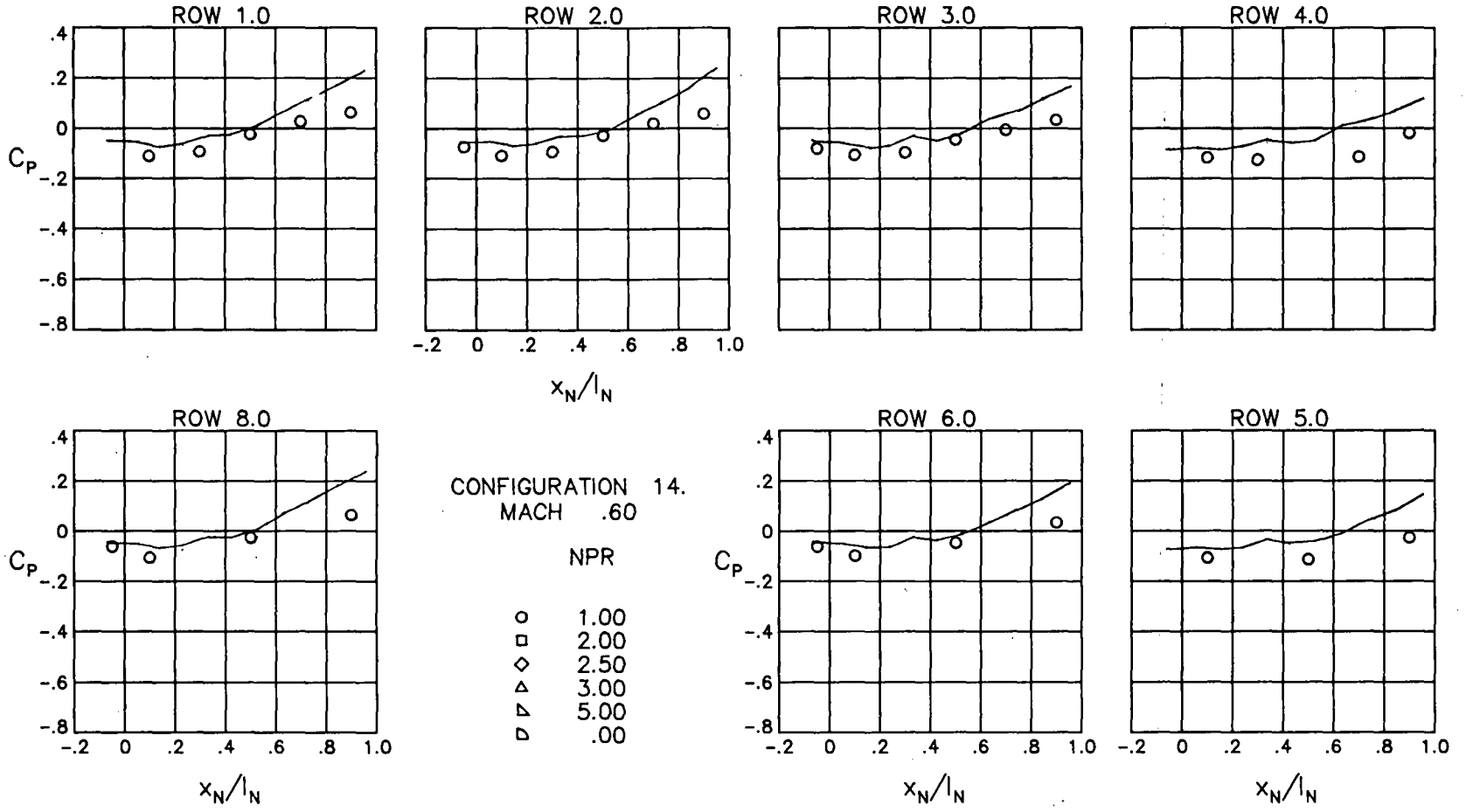

(d) Configuration 14.

Figure 6.- Continued.

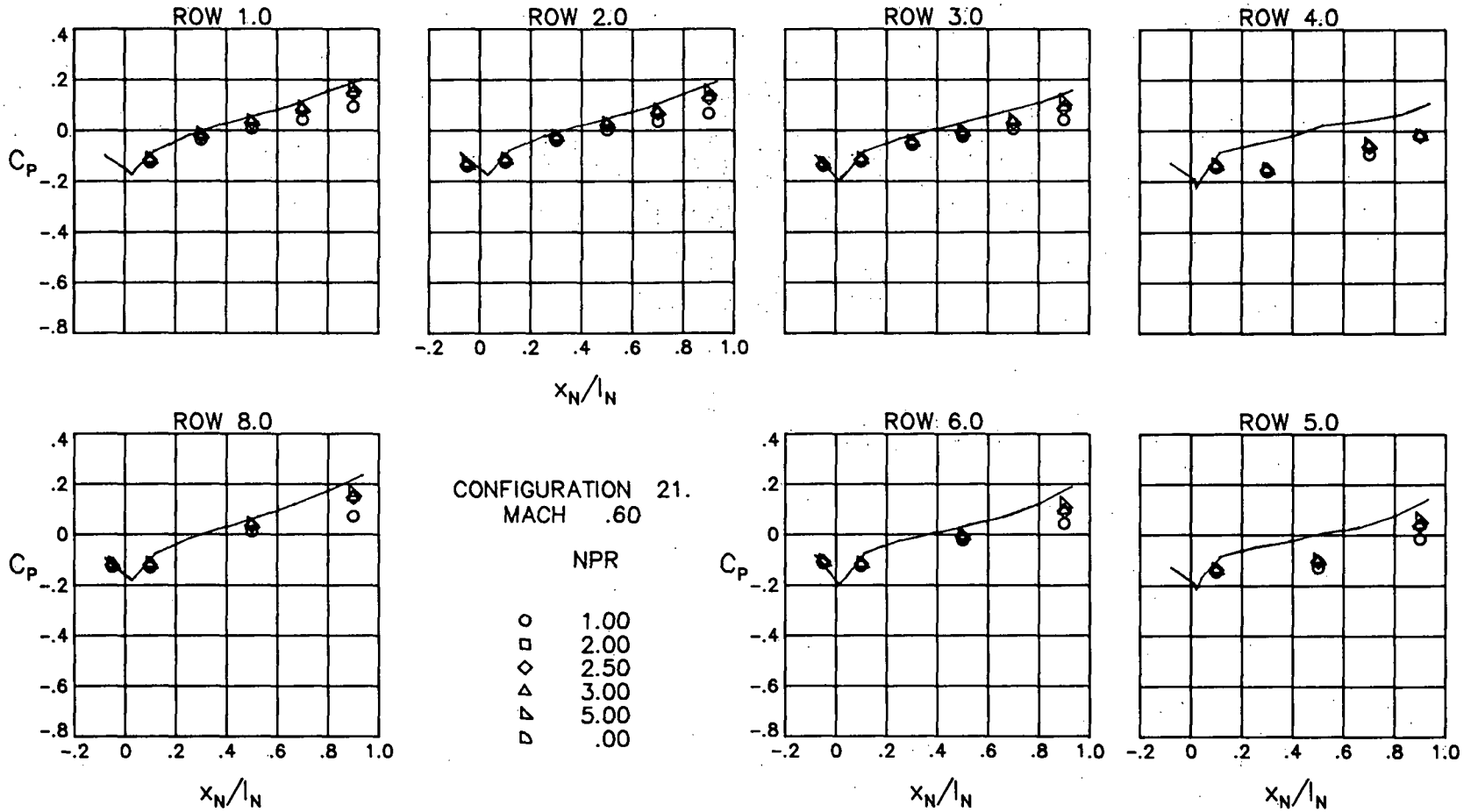

(e) Configuration 21.

Figure 6.- Concluded.

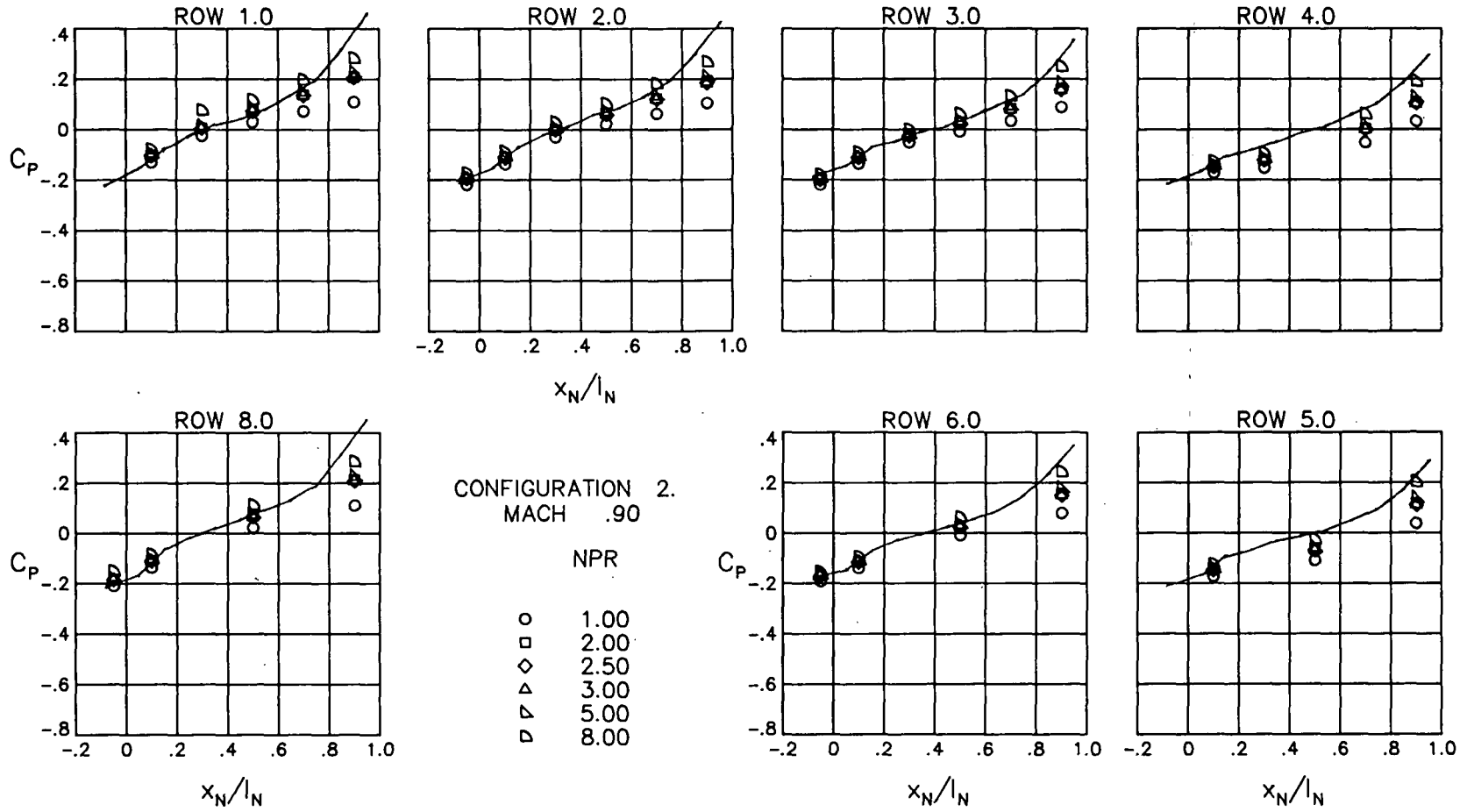

(a) Configuration 2.

Figure 7.- Surface static pressure coefficient distributions around the nozzles at M = 0.90 and $\alpha = 0^{o}$. Solid lines represent the computed values.

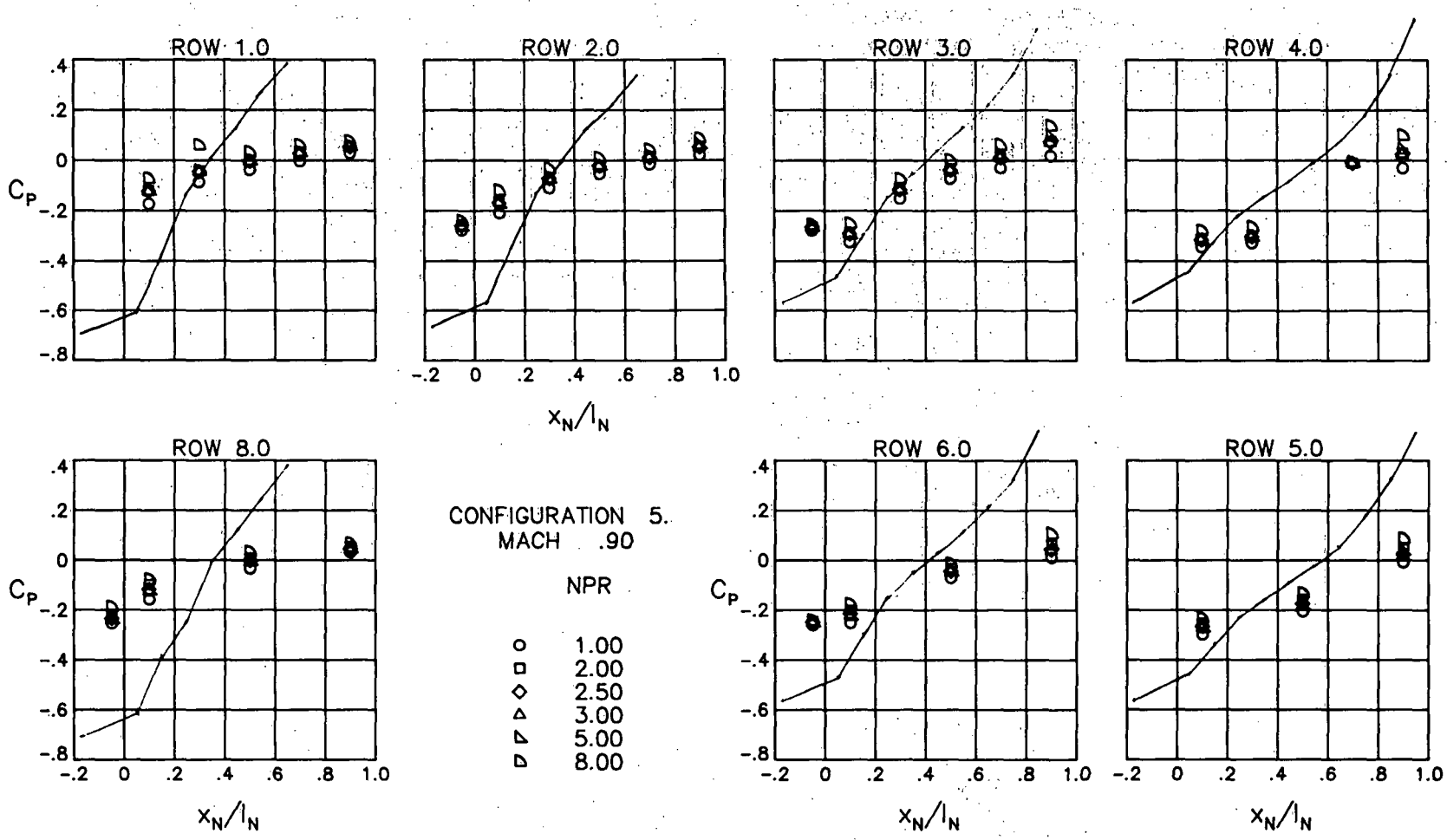

(b) Configuration 5.

Figure 7.- Continued.

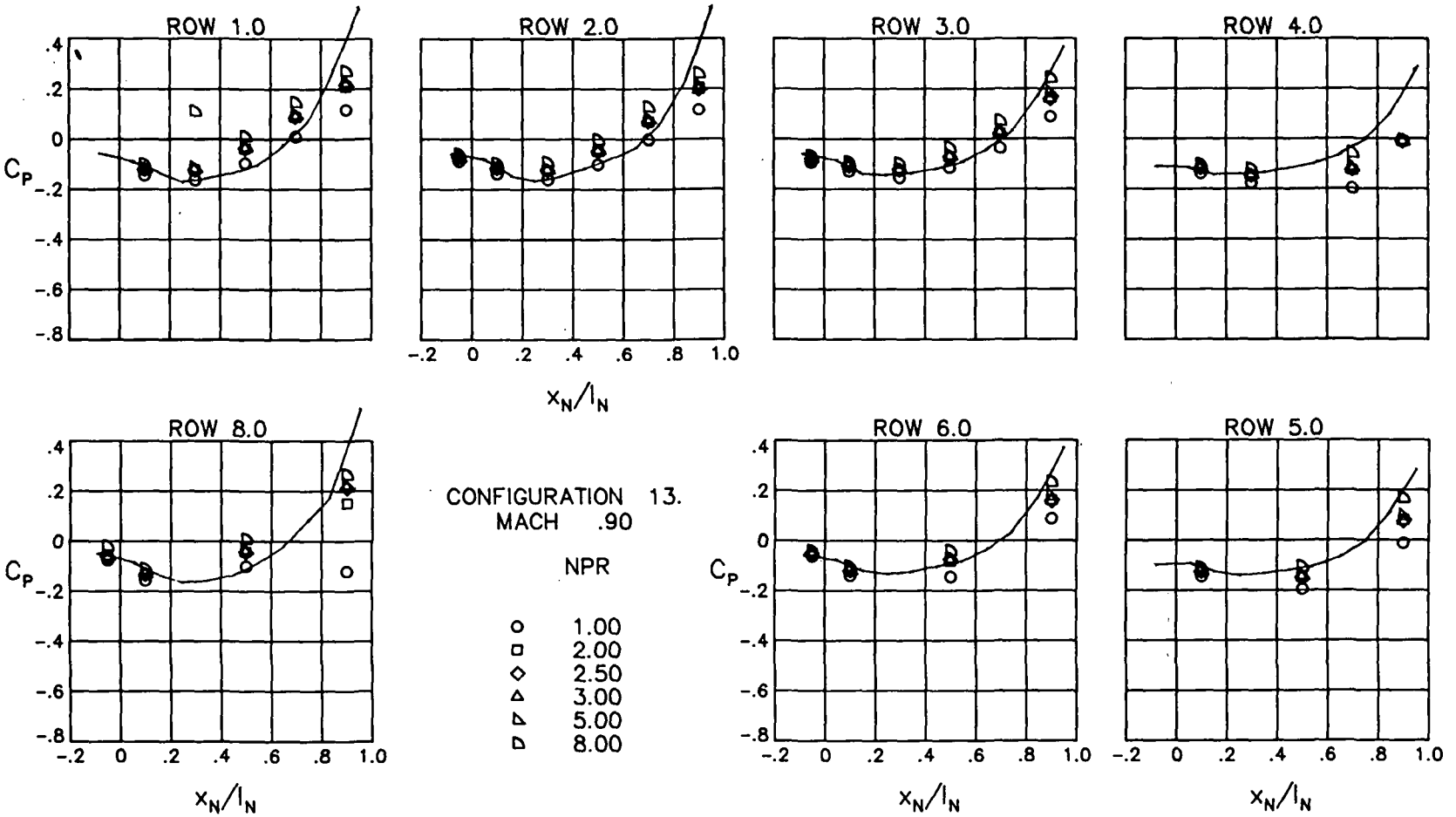

(c) Configuration 13.

Figure 7.- Continued.

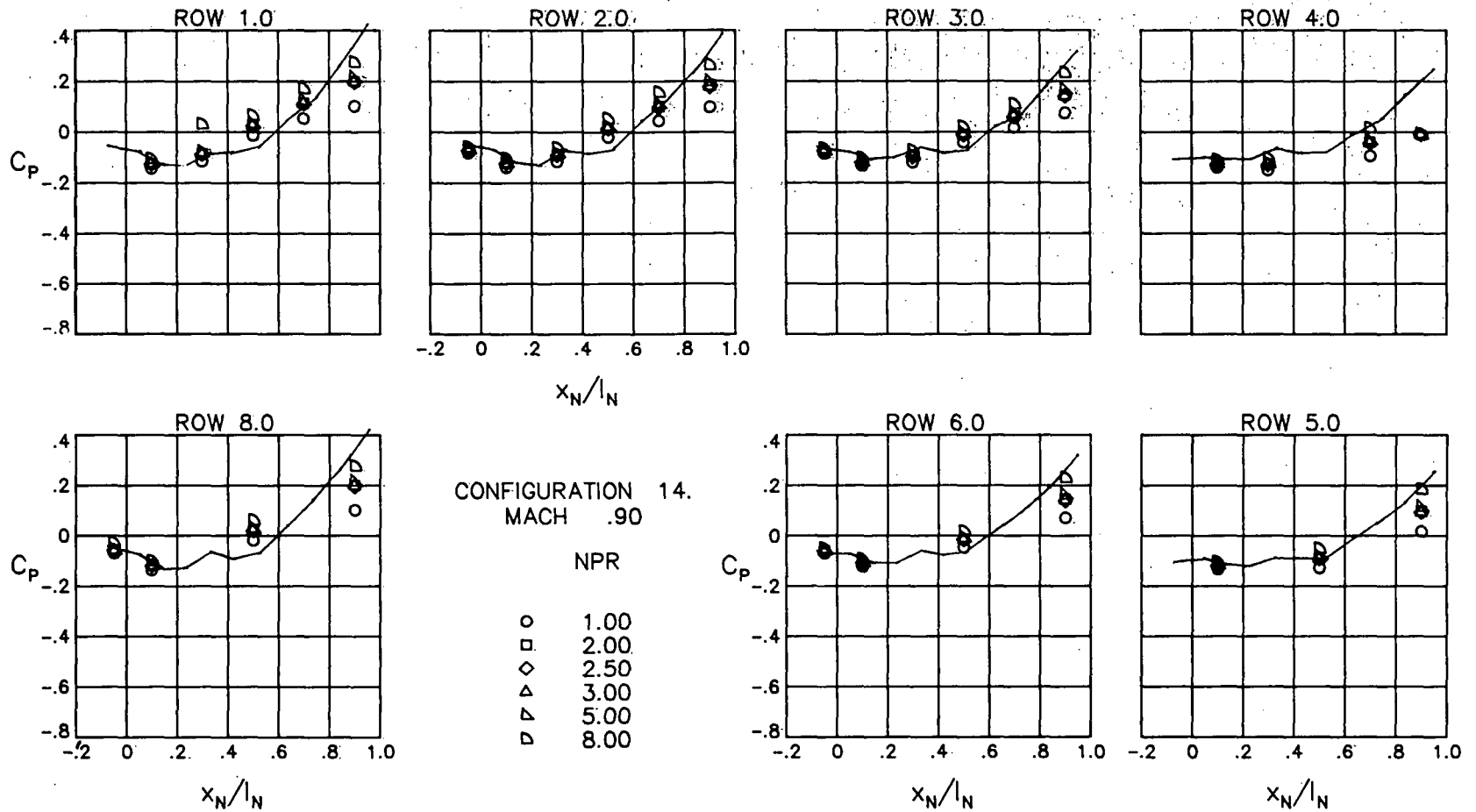

(d) Configuration 14.

Figure 7.- Continued.

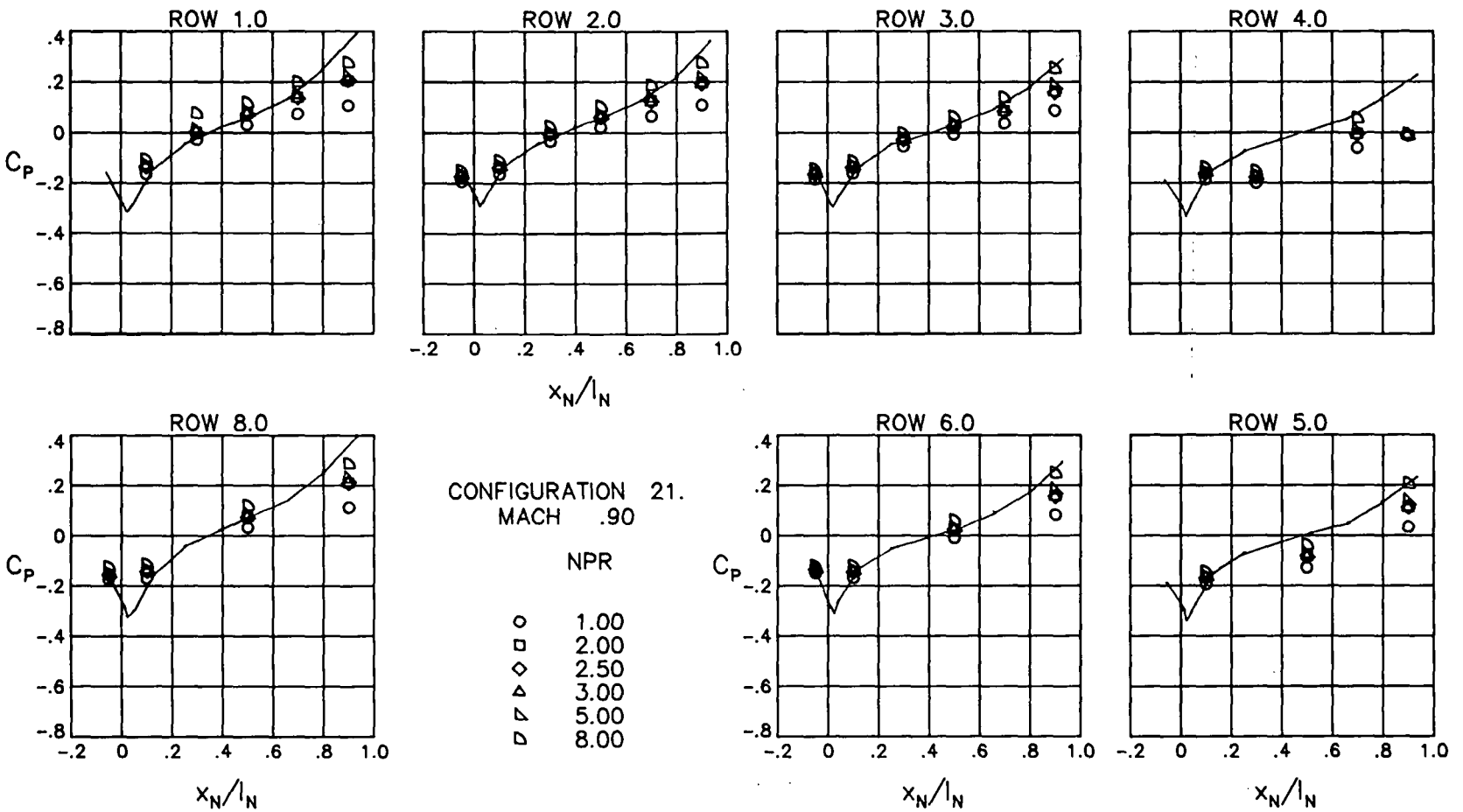

(e) Configuration 21.

Figure 7.- Concluded.

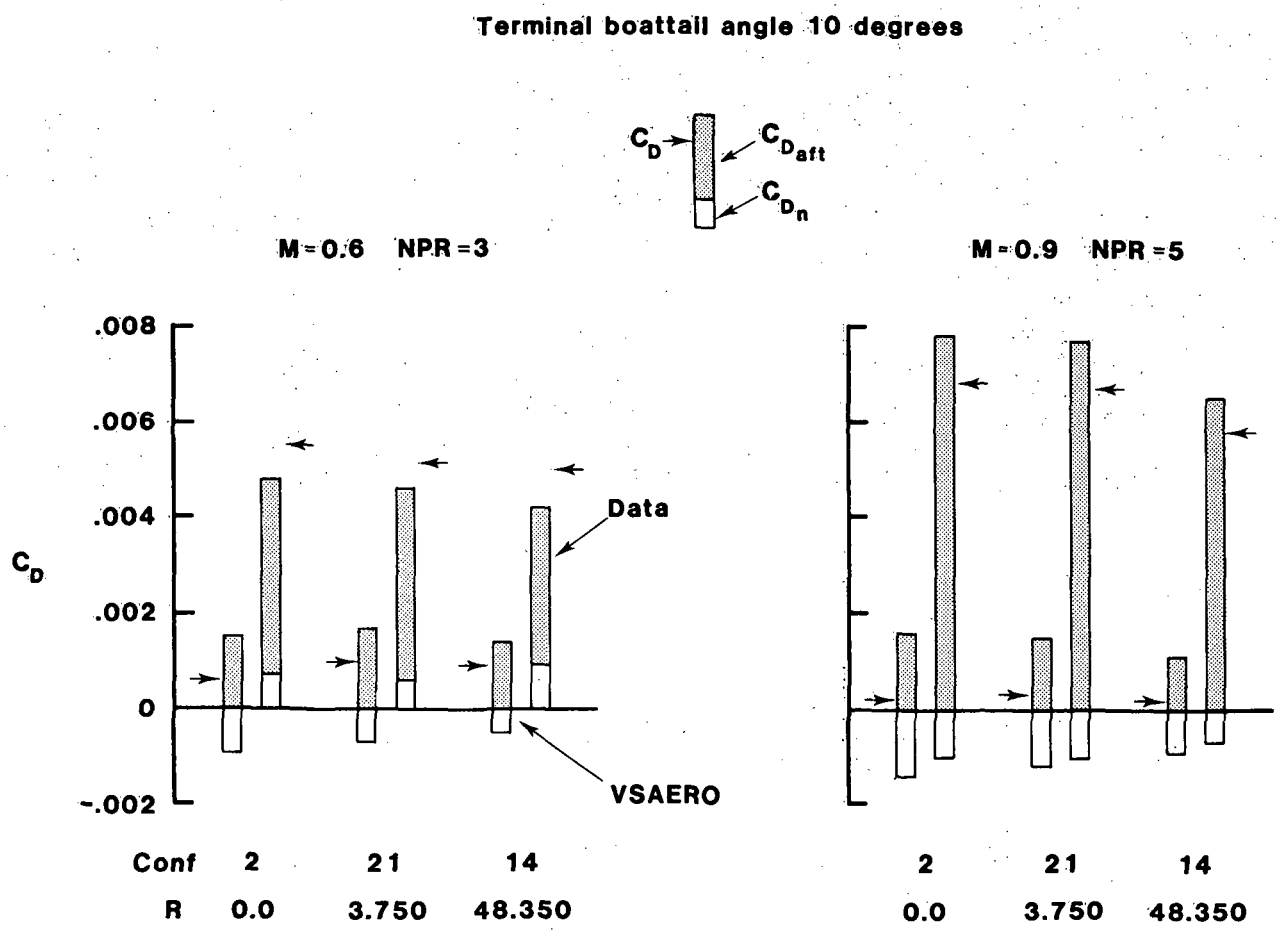

Figure 8.- Comparison of theoretically predicted afterbody/nozzle drag coefficient and experimental drag coefficient for $\beta_t = 10^0$, at M = 0.60 and 0.90, and $\alpha = 0^0$.

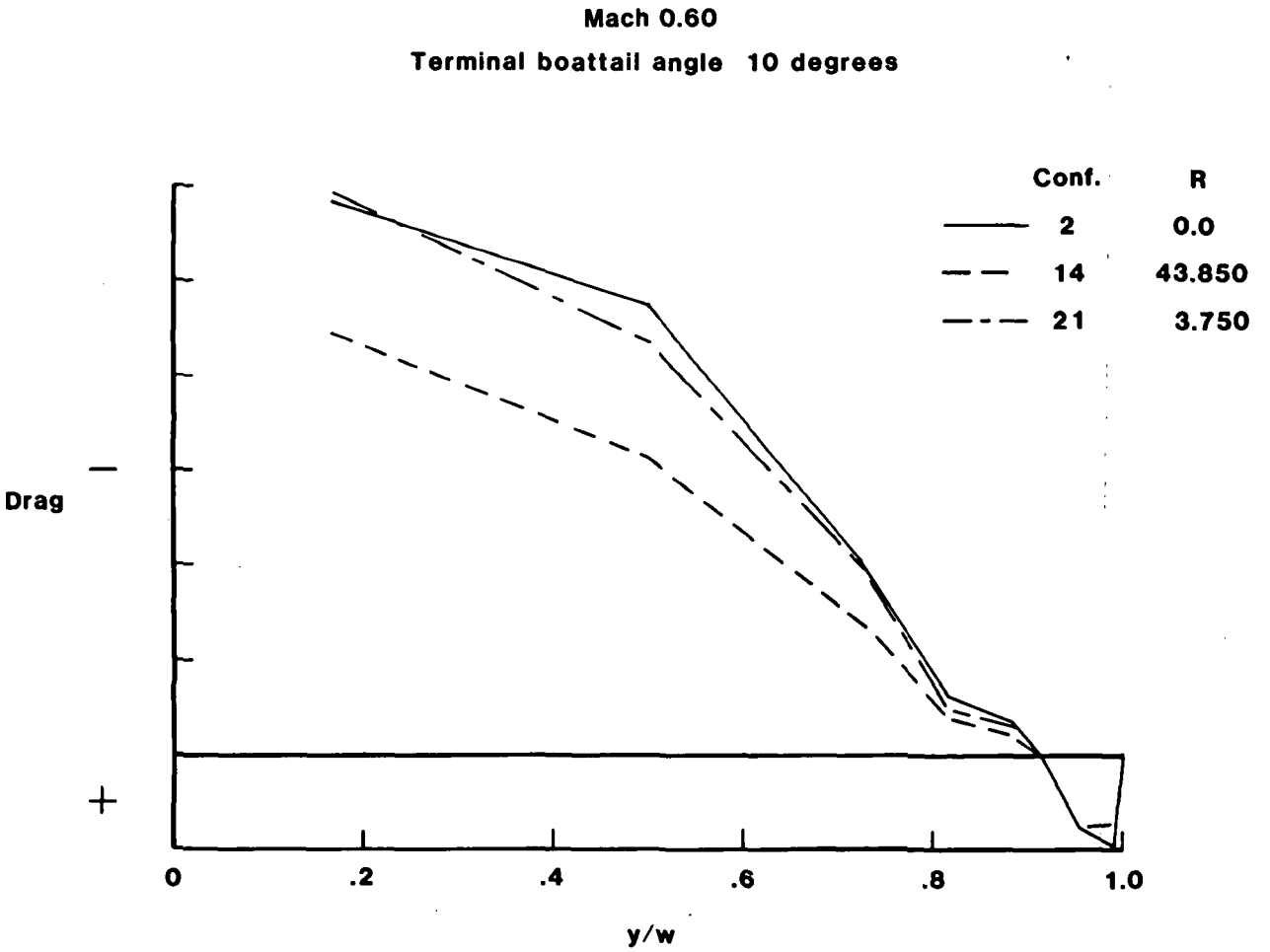

Figure 9.- Theoretical prediction of spanwise integrated pressure drag coefficient for M = 0.60 and $\alpha = 0^{o}$.

Standard Bibliographic Page

1. Report No.	2. Government Accession No.	3. Recipient's Catalog No.
NASA TM-87757		

4. Title and Subtitle	5. Report Date
COMPARISON OF EXPERIMENTAL SURFACE PRESSURES WITH THEORETICAL PREDICTIONS ON TWIN TWO-DIMENSIONAL CONVERGENT-DIVERGENT NOZZLES	August 1986
	6. Performing Organization Code: 505-62-91-01
7. Author(s): John R. Carlson, Odis C. Pendergraft, Jr., and James R. Burley, II	8. Performing Organization Report No.
9. Performing Organization Name and Address: NASA Langley Research Center, Hampton, VA 23665	10. Work Unit No.
	11. Contract or Grant No.
12. Sponsoring Agency Name and Address: National Aeronautics and Space Administration, Washington, DC 20546	13. Type of Report and Period Covered: Technical Memorandum
	14. Sponsoring Agency Code

15. Supplementary Notes

This paper was presented at the AIAA 4th Applied Aerodynamics Conference, June 9-11, 1986, in San Diego, California. AIAA Paper No. 86-1803-CP.

16. Abstract

A three-dimensional subsonic aerodynamic panel code (VSAERO) was used to predict the effects of upper and lower external nozzle flap geometry on the external afterbody/nozzle pressure coefficient distributions and external nozzle drag of nonaxisymmetric convergent-divergent exhaust nozzles having parallel external sidewalls installed on a generic twin-engine high performance aircraft model. Nozzle static pressure coefficient distributions along the upper and lower surfaces near the model centerline and near the outer edges (corner) of the two surfaces were calculated, and nozzle drag was predicted using these surface pressure distributions. A comparison between the theoretical predictions and experimental wind tunnel data is made to evaluate the utility of the code in calculating the flow about these types of non-axisymmetric afterbody configurations.

For free-stream Mach numbers of 0.60 and 0.90, the conditions where the flows were attached on the boattails yielded the best comparison between the theoretical predictions and the experimental data. For the boattail terminal angles of greater than 15°, the experimental data for M = 0.60 and 0.90 indicated areas of separated flow, so the theoretical predictions failed to match the experimental data. Even though calculations of regions of separated flows are within the capabilities of the theoretical method, acceptable solutions were not obtained.

17. Key Words (Suggested by Authors(s))	18. Distribution Statement
Aerodynamics Propulsion integration Theoretical method	Unclassified - Unlimited Subject Category 02

19. Security Classif.(of this report)	20. Security Classif.(of this page)	21. No. of Pages	22. Price
Unclassified	Unclassified	30	A03

For sale by the National Technical Information Service, Springfield, Virginia 22161